Journal of Materials Science: Materials in Electronics (2018) 29:15649–15657
https://doi.org/10.1007/s10854-018-9160-7

Study of the effect of the synthesis temperature on the photoluminescent properties of InP@ZnS nanocrystals

F. Angel-Huerta[1] · M. P. González-Araoz[2] · J. S. Arias-Cerón[3] · J. F. Sánchez-Ramírez[4] · J. Díaz-Reyes[4] · J. L. Herrera-Pérez[1] · J. G. Mendoza-Álvarez[5]

Received: 17 November 2017 / Accepted: 21 April 2018 / Published online: 28 April 2018

Abstract
In this work reports the synthesis and the characterization of InP@ZnS nanocrystals prepared by the colloid chemistry method at different synthesis temperatures. Varying the reaction temperature from 100 to 320 °C was possible to control the formation of the ZnS-shell on InP nanocrystals. The results of the nanocrystals chemical composition obtained by energy-dispersive X-ray spectroscopy demonstrated that with the increase of the reaction temperature the particles are obtained with a better stoichiometric ratio. By X-ray diffraction analysis and Raman scattering reveal that semiconductor nanocrystals showed the zinc blende crystalline phase in the direction (111), which was confirmed by high resolution transmission electron microscopy. The average nanocrystals sizes (2–10 nm) were estimated by the Wang equation, which are confirmed analysing the grain average diameter by transmission electron microscopy measurements. The nanocrystal sizes indicate a high quantum confinement because of they are lower than the InP exciton Bohr radius. The obtained semiconductor nanocrystals presented crystalline structure InP-core@ZnS-shell, uniformity in size and exhibit a dependence of emission in the range from 450–650 nm measured by UV–Vis spectroscopy, which allowed obtaining the bandgap of the nanostructures. The bandgap energy could be tuned from 3.73 to 2.38 eV through the variation of the synthesis temperature. The emission peak in InP-core varied as a function of quantum dots size, ranged in the 2.61–2.17 eV region. The InP@ZnS nanocrystals present a high passivation for samples synthetized at 300 °C.

1 Introduction

II–VI semiconductor nanocrystals (NCs) are a class of materials with unique optical properties; they are of considerable interest for both fundamental research and technological applications [1–5]. Among the family of II–VI semiconductors, ZnS [6, 7], CdSe [8], ZnO [9], CdTe [10], and others, are the foremost candidates because of their favourable electronic and optical properties for optoelectronic applications [11]. CdSe and CdTe are ones of the most interesting materials due to their strong luminescence in the visible spectral range, wide band gap and large exciton binding energy at room temperature [1–3]. However, the applications of the mentioned semiconductor NCs are problematic due to the intrinsic toxicity of cadmium. One of the alternative choices for Cd-free semiconductor NCs with similar emission properties is InP. InP nanoparticles with null or weak luminescence have been prepared based on both top–down and bottom–up approaches with proper control of nanoparticles form and dispersion, besides restricting their size at nanometer

✉ J. Díaz-Reyes
joel_diaz_reyes@hotmail.com

1 Unidad Profesional Interdisciplinaria en Ingeniería y Tecnologías Avanzadas, Instituto Politécnico Nacional, Av. Instituto Politécnico Nacional No. 2580. Col. Barrio la Laguna Ticomán, 07340 México City, Mexico

2 Facultad de Ingeniería, Benemérita Universidad Autónoma de Puebla, Boulevard Valsequillo s/n, Ciudad Universitaria, 72570 Puebla, Puebla, Mexico

3 Departamento de Ingeniería Eléctrica, SEES, Centro de Investigación y de Estudios Avanzados del Instituto Politécnico Nacional, Apdo. Postal 14-740, 07000 México City, Mexico

4 Centro de Investigación en Biotecnología Aplicada, Instituto Politécnico Nacional, Ex–Hacienda de San Juan Molino. Km 1.5 de la Carretera Estatal Santa Inés Tecuexcomac-Tepetitla, 90700 Tepetitla, Tlaxcala, Mexico

5 Departamento de Física, Centro de Investigación y de Estudios Avanzados, Instituto Politécnico Nacional, Apdo. Postal 14-740, 07000 México City, Mexico

scale [7, 10, 12, 13]. However, few methods have the capacity to produce InP nanoparticles encapsulated with other material to stabilize and improve their unique optical properties, their preparation is non-trivial. InP is a direct bandgap binary semiconductor with a bandgap energy of 1.344 eV at room temperature [14] and exhibits quantum size effects and size-dependent optical spectra at nanometer scale. Making it of considerable interest for applications in laser devices [15], fluorescent probes for biomedical applications, as light emitters or absorbers in optoelectronic devices such as light emitting diodes and solar cells. After appropriate surface treatments, e.g., with HF etching [16] or by overgrowth with a ZnS shell [16–18], InP NCs can become highly luminescence materials. Using the steady-state photoluminescence (PL) technique, the overall PL spectra generally show various spectral components originating from different radiative recombinations/transitions. The PL intensity of each spectral component depends on the corresponding recombination/transition rate and its density of states. When looking at the PL spectra of InP@ZnS (InP-core/ZnS-shell) NCs in the literature, only the emission component of InP has been reported. It is clearly showed the quantum size effect with the PL wavelength varying from green to near infrared as the core-InP NCs size increased from around 2 to 6 nm [17–19]. The observed high fluorescence quantum yield (Q.Y.) also showed that an efficient passivation of trap states was achieved by the ZnS-shell. It has been reported that the InP nanoparticles without ZnS shell do not emit and that the shell has no radiative transitions [11].

Based on the background and with the goal of having a control on the formation and the luminescent properties of the InP nanocrystals. It reports in this article the results of the controlled synthesis of InP semiconductor nanostructures with ZnS surface passivation obtained by single-step procedure without precursor injection [4]. It also is presented a systematic study on optical properties of ZnS-shell formation on InP nanoparticles dependent of the synthesis temperature. The different physical properties of InP@ZnS were characterized and studied using several techniques such as energy dispersive spectrometry (SEM–EDS), transmission electron microscope (TEM) and high resolution TEM (HR-TEM), UV–Vis absorption and PL spectroscopies.

2 Materials and methods

2.1 Materials

All reagents and solvents were purchased from Sigma-Aldrich and used as received: indium acetate (99.99%), zinc stearate (90%), myristic acid (> 99%), tris(trimethylsilyl) phosphine (95%), 1-dodecanethiol (DDT) (97%), 1-octadecene (90%). HPLC water was used in all times to wash the laboratory equipment used in the preparation of the samples.

2.2 Synthesis of InP@ZnS nanocrystals

For the synthesis of semiconductor nanocrystals, the chemical method proposed by Li and Reiss [4] with slight modifications was used. In general, the single-step procedure without precursor injection involves the simultaneous mixture of all molecular precursors at an inert atmosphere of argon at room temperature and then heated at high temperatures. In this work, a precursors atomic ratio of In:P:Zn:S = 1:1:1:1 was used and at different reaction temperatures (T_s = 100, 150, 200, 250, 300 and 320 °C) to control the formation of the ZnS-shell on InP nanocrystals. The results are shown in Table 1. Under these experimental conditions, it was observed that all the reagents reacted to form semiconductor nanoparticles. The in situ formation of the InP@ZnS nanocrystals is associated to the difference of the activation energy of reagents [20]. For the synthesis temperature of 100 °C, it was observed that the DDT reacts to form ZnS on InP-core and with the temperature increase at 320 °C; its chemical reactivity was enhanced by increasing the amount and stoichiometric quality of ZnS on the surface of InP core. The nanocrystals were then purified with a chloroform/methanol/acetone (1:1:10 in volume) mixture

Table 1 It presents the In, P, Zn and S concentrations of the InP@ZnS samples synthetized and studied in this work, which were estimated by SEM–EDS (mean values of five independent measurements per sample)

Sample	T_s (°C)	In mass fraction (%)	In molar fraction (%)	P mass fraction (%)	P molar fraction (%)	Zn mass fraction (%)	Zn molar fraction (%)	S mass fraction (%)	S molar fraction (%)
M1	100	59.03	37.54	8.28	19.52	27.16	30.33	5.54	12.61
M2	150	48.41	27.67	11.40	24.15	32.65	32.76	7.54	15.42
M3	200	50.07	27.16	15.36	30.90	25.48	24.27	9.09	17.67
M4	250	48.10	25.88	12.28	24.49	27.23	25.73	12.40	23.89
M5	300	47.21	25.05	12.65	25.08	26.78	25.10	13.36	24.77
M6	320	45.63	24.78	13.31	26.82	26. 05	24.85	12.11	23.55

followed by centrifugation to remove the starting materials and side products. The InP@ZnS NCs chemical stoichiometry was estimated by SEM–EDS, which was carried out in a System LEO 438VP, with W.D. of 26 mm using a pressure of 20 Pa. The crystalline phase and structure of the nanocrystals were determined with a Bruker D8 Discover diffractometer using the copper Kα radiation (λ = 1.5406 Å) at 40 kV and 40 mA with parallel beam geometry. High-resolution transmission electron microscopy (HRTEM) studies were carried out in a JEOL JEM200 of 80–200 kV; the obtained images are recorded with a CCD camera in real time. The Gatan Digital Micrograph software was used for the analysis of HRTEM images. High-resolution electron microscope (HRTEM) images were digitally processed by using filters in the Fourier space. For electron microscopy analysis, two microscopes, a Jeol JEM200 and a Tecnai 200 TEM, were used for the low-magnification and high-resolution observations of the samples, respectively. Room temperature optical absorption spectra of the colloidal samples were recorded using a 10 mm path length quartz cuvette in a UV–Vis–NIR scanning spectrophotometer (Shimadzu UV 3101PC double beam). The PL was measured using a He–Cd (Omnichrome—Series 56) laser emitting at 325 nm with an optical excitation power of 15 mW at room temperature. The radiative emission from the sample was focalized to the entrance slit of a HRD-100 Jobin–Yvon double monochromator with a resolution better than 0.05 nm, and detected with an Ag–Cs–O Hamamatsu photomultiplier with a spectral response in the range 350–1000 nm.

3 Results and discussions

In order to determine of the structural properties of the obtained nanocrystals, XRD analysis and Raman scattering of typical samples were performed. Figure 1 shows the XRD patterns of two typical InP@ZnS NCs obtained varying the synthesis temperature, 100 and 150 °C, which correspond to the samples M1 and M2. It is observed from XRD patterns that synthesised InP@ZnS NCs are in polycrystalline nature. As can be seen, the XRD patterns of the samples show clearly a predominant peak at $2\theta = 26.27°–26.30°$, which can be assigned to (111) plane of zinc blende InP crystalline phase, FCC, with an interatomic distance of 3.39 Å, indicating a preferential growth orientation. In addition, it can be seen that each peak corresponds fairly well with data of InP marked in the software JCPDS PDF No. 32-452 data. Another peak observed at range 30.34°–30.37° is indexed as the ZB (200) diffraction plane. It is important to mention that in XRD patterns the presence of the ZnS shell is not detected, which is indicative that ZnS shell is very thin; of the order of 4 or 5 atomic layers as has been reported [21]. The lattice constants of InP NCs zinc blende

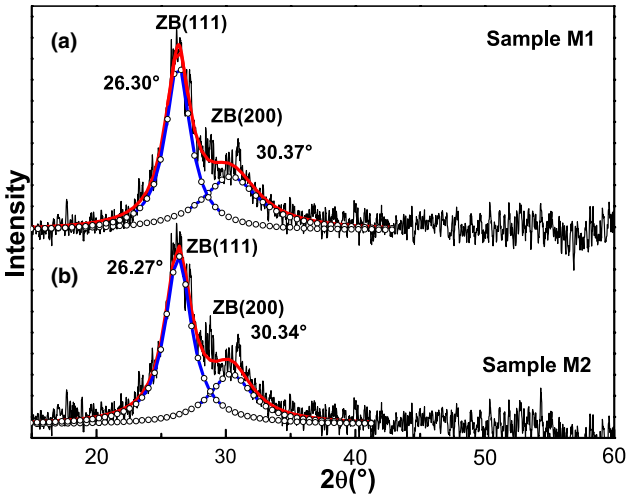

Fig. 1 XRD patterns of two typical as-prepared InP@ZnS NCs synthetized at different temperatures: M1 (100 °C) and M2 (150 °C). It shows the diffractograms that display a peak at $2\theta = 26.30°–26.27°$. This is related to the (111) diffraction plane for the ZB crystalline phase of the InP

crystalline phase were $a = 5.8575 \pm 4 \times 10^{-4}$ Å (Fig. 3a) and $5.8677 \pm 8 \times 10^{-4}$ Å (Fig. 3b), both are close to standard data (JCPDS PDF No. 32-452, $a = 5.869$ Å). According to the Full Width at Half Maximum of the dominant diffraction peak (111) observed at 26.27°–26.30°, and using the Debye–Scherrer formula, the mean crystalline sizes of the nanocrystals synthesised at different temperatures were about 3.51 and 5.31 nm, respectively, which are presented in Table 2. Figure 2 shows the Raman spectrum of the typical InP@ZnS NCs obtained after a synthesis temperature of 150 °C, sample M2, using the 6328 Å line of a He–Ne laser at normal incidence as the excitation source. The Raman spectrum shows two vibrational peaks at 304 and 339 cm^{-1}, which are associated at transverse optical (TO) and longitudinal optical (LO) phonon lines corresponding to the zinc blende crystal structure of the InP NCs and are clearly resolved [22, 23]. It is noteworthy that both the TO and LO Raman scattering lines can be observed because the NCs are randomly oriented; that is different from the case of oriented bulk InP, in which the recorded Raman spectrum depends on the lattice facets under measurement respecting the Raman scattering selection rule, which confirms that preferential growth direction is (111). The LO phonon frequency exhibits a distinct redshift, as shown in Fig. 2. This observation can be explained by the quantum confinement effect of phonon modes associates to nanocrystal size [22]. In addition, a weak peak is observed at 691 cm^{-1} that is associated to 2LO. By comparing of the 2LO and LO intensities to the reported size-dependent Raman spectra, it estimates the size of the InP NCs to be of 3–4 nm [22, 24], which is in good agreement with the crystallite size estimated from XRD

Table 2 Variation of particle size and bandgap energy of InP@ZnS synthesised at different temperatures and comparing the average grain sizes estimated by the three experimental techniques

Sample	Band gap (eV)	FWHM (meV)	Particle size from Wang equation (nm)	Particle size from TEM (nm)	Particle size from X-ray (nm)
M1	3.73	348.5	3.28	3.22	3.51
M2	2.67	219.9	4.04	4.25	4.03
M3	2.53	199.2	4.19	4.63	4.74
M4	2.42	192.1	4.33	4.83	5.10
M5	2.38	177.8	4.37	5.11	5.32
M6	2.39	178.2	4.38	6.57	5.31

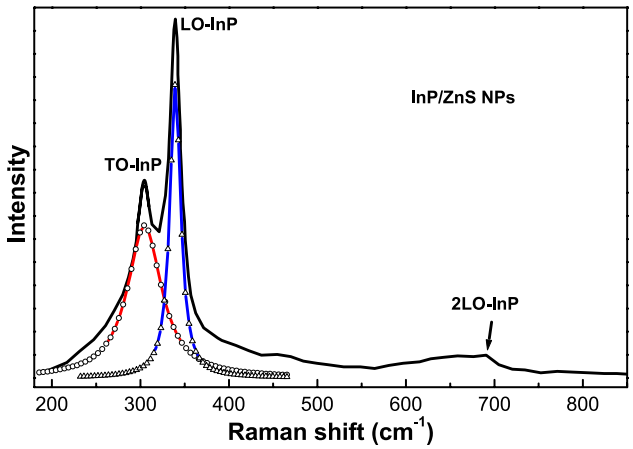

Fig. 2 Raman scattering spectrum of the obtained InP NCs (synthesis temperature 150 °C). Its mean size of ~3–4 nm is estimated from the Raman shift and the intensity ratios between the 2LO and LO lines

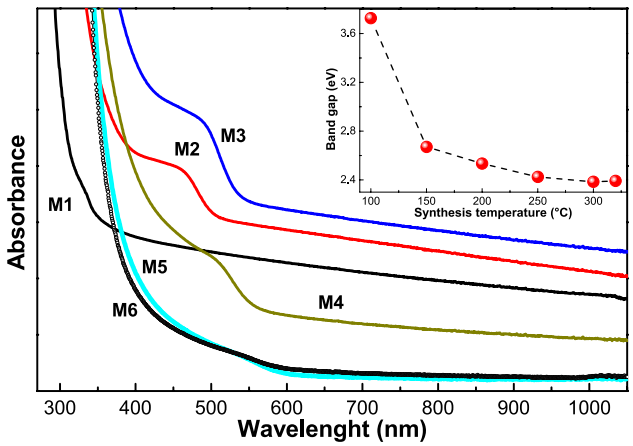

Fig. 3 Room temperature absorption spectra of InP@ZnS NCs synthesized at different temperatures. The inset illustrates the variation of bandgap energy as function of the synthesis temperature

measurements. On the other hand, no Raman peak associated with ZnS is detected, which is indicative that the shell is very thin, confirming the previous results.

The chemical composition of the InP@ZnS nanocrystals was estimated by EDS. The results of these measurements are shown in Table 1, in which the atomic mass and percentages are included. From the analysis of these results is observed that at low synthesis temperatures the obtained nanoparticles are not stoichiometric, both the InP-core and the ZnS-shell. For example, for synthesis temperature of 100 °C the sample presents final ratios of In:P = 1.9:1.0 and Zn:S = 2.4:1.0, as is observed there is a high presence of In and Zn accompanied by greater absence of P and S. The average errors with that were calculated percentage masses of the different elements were for indium 0.73%, phosphorus 0.26%, zinc 0.41% and for sulphur 0.25%; these errors do not alter significantly the findings results. For higher reaction temperatures, the nanoparticles are obtained with a better stoichiometry ratio. At 300 °C synthesis temperature, the nanoparticles are obtained with approximate stoichiometric ratios of 1.0:1.0, for both InP and ZnS. Since the unit cell corresponds to zinc blende, so considering that each unit cell of InP-core and ZnS-shell contains four atoms. Therefore, the atomic weight of the ideal unit cell of InP corresponds to 78.8% indium atoms and 21.2% phosphorus atoms, and for ZnS corresponds to 72.7% zinc atoms and 27.29% sulphur atoms. Then, when a stoichiometric composition deviation of ideal unit cell occurs, it could be established a correspondence between vacancies or interstices of some of the constituent chemical elements in the synthesized samples. At temperatures below 250 °C the synthesized samples present an excess of In and Zn accompanied by a lack of P and S, which is indicative that In and Zn are interstitial and there are vacancies of P and S.

The effects of synthesis temperature on the optical properties of the InP@ZnS nanocrystals, including percentage of absorbance (percentage of A) and bandgap energy (E_G), which are studied in detail and the obtained results are presented in Fig. 3. It is well known that nanocrystals of semiconductor materials, such as InP, in the nanometric scale strongly absorb light when the excitation energy is greater than the bandgap energy, during this process, electrons are promoted from the valence band to the conduction band, these electronic energy states may be quantified

with measurements of UV–Vis spectroscopy. The lowest excited energy state is shown by the first observable peak in the absorption spectrum, which is known as the quantum-confinement peak. The energy of the quantum-confinement peak depends on the size, shape and structure type (core@shell) [25]. The absorbance spectra in the visible and infrared ranges are recorded for the InP-ZnS nanocrystals synthesized at different temperatures in the wavelength range 270–1050 nm. It is evident from Fig. 3 that samples exhibit a strong absorption at wavelength range 335–522 nm suggesting blue shift w.r.t. the bulk InP arising from quantum-confinement effect in the nanocrystals. As is observed from Fig. 3, the InP@ZnS NCs absorption edge shifts slightly towards long wavelengths as the synthesis temperature (T_S) is increased, this might be indicative the ZnS shell formation on InP with increasing T_S. This observation is attributed to a partial leakage of the excitation into the shell [26]. On the other hand, the optical band gap (E_G) of a semiconductor is related to the optical absorption coefficient (α) and the incident photon energy ($h\nu$). In order to quantify the optical band gap (E_G) of the samples, the optical absorption coefficient (α) of nanocrystals was obtained. The E_G was then evaluated from the absorbance spectrum using the Tauc relation [27–29]: $\alpha h\nu = \left(E_G - h\nu\right)^n$, where n depends on the kind of optical transition that prevails. Specifically, n is 1/2 and 2 when the radiative transition is directly and indirectly allowed, respectively. The InP is known to be a semiconductor with a direct allowed transition. The InP@ZnS average optical band gap energies, which were estimated from the linear portion of the $(\alpha h\nu)^2$vs $h\nu$ graphic, using the Tauc graphics, which are shown the obtained results in Table 2 and inset of Fig. 3 [30]. It is observed that the band gap energies of the semiconductor nanocrystals were higher than the value of bulk InP at room temperature (1.344 eV) [14]. The optical cut-off energy shows a blue shift from 1.04 to 2.38 eV, which is indicative of a high quantum confinement of nanoparticles that confirms the formation of InP nanocrystals. The optical bandgap energy of the sample M1, which was synthetized at 100 °C, is of 3.24 eV. This value is the highest of all the synthesized samples, it maybe associated to the formation of InP-core@ZnS-shell nanocrystals and possibly at the beginning of the formation of the ZnS shell [11]. In the inset of Fig. 3, the variation of the bandgap energy of the samples as a function of synthesis temperature is shown, in which is observed that from 150 °C the variation of the bandgap is small and it is slightly redshifted. This might mean that the size of the semiconductor nanocrystals is homogenized and the decrease of the band gap energy is due to its slight size increase. In order to determine the average particle size of InP nanocrystals in the system core@shell the Wang equation was also used [31, 32]:

$$E_{GNP} = E_{Gbulk} + \frac{\hbar^2\,\pi^2}{2r^2\mu^*} - \frac{1.786e^2}{\epsilon_r\epsilon_0 r}$$

where E_{GNP} is the band gap energy of the InP nanocrystals, E_{Gbulk} is the band gap energy of bulk InP, $r = d_{ab}/2$ is the diameter of the nanocrystals, and ϵ_r is the permittivity of nano InP and the rest of the parameters have already been defined elsewhere. The effective mass μ^* is defined as $1/\mu^* = 1/2(1/m_e^* + 1/m_h^*)$. For InP $m_e^* = 0.08m_0$ and $m_h^* = 0.6m_0$ and $\epsilon_r = 12.5$ is the InP dielectric constant [14]. The calculated nanoparticle sizes are presented in Table 2.

The TEM measurements of the synthesized samples corroborate the presence and the nanometric size of the particles. In Fig. 4a is shown a TEM micrograph of the sample synthesised at 320 °C, it is evident the presence of particles with almost completely spherical shape. Based on

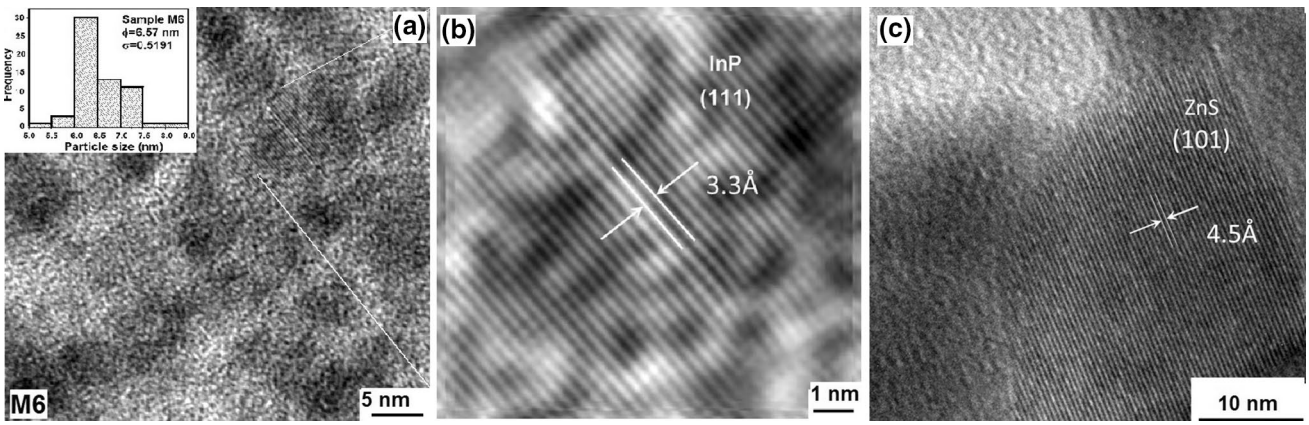

Fig. 4 **a** It shows the typical TEM micrograph of the semiconductor nanocrystals and the inset illustrates its respective size distribution histogram, **b** HRTEM image showing the lattice fringes of InP@ZnS nanocrystals obtained of sample M6 and **c** HRTEM image of single ZnS nanocrystals synthetized at 280 °C

more than 100 measurements taken from the TEM micrographs of the samples a size distribution histogram was obtained, and it can be detected a Gaussian adjustment with a narrow distribution of size and a maximum value of 6.5 nm. Absence of bimodal size distribution in the size distribution histograms suggests that the nanoparticles obtained by our synthesis process at different temperatures corresponds to the formation of an InP–ZnS system and not the physical mixture of individual nanoparticles of InP and ZnS. A comparable analysis was performed for the rest of the samples and the results are listed in Table 2. Bigger semiconductor nanocrystals are obtained with the increase of the reaction temperature. Therefore, the reaction temperature can use to control the formation and size of the InP@ZnS nanocrystals. As can be seen in Table 2, the particle size values obtained by the Wang equation, through of the band gap energy obtained from the absorption measurements and those measured from the TEM micrographs have slight discrepancy. These small discrepancies in particle size is due to some approximations involved in the calculations using the Wang equation (with the band gap value 1.344 eV of bulky zinc blende InP) or coalescence of nanocrystals during preparation for TEM analysis. In addition, this could be due to the fact that for TEM measurements one should deposit the NCs colloidal solution on the microscope grids and to wait until the solvent evaporates. It is possible that in this process could be some coalescence of the nanoparticles, in such a way that when these are observed in the TEM, they have already increased their size. As expected, increasing the reaction temperature from 100 to 320 °C causes a large redshift due to the crystal growth of the as-prepared products. These phenomena were likely due to the quantum-confinement effect of the as-synthesized InP nanocrystals, whose diameters are several nanometres smaller than the InP exciton Bohr radius that is 15 nm [33], as can be seen in Table 2. With the aim to verify the structure's quality and crystalline phase of the obtained semiconductor nanocrystals, HRTEM images were taken and the results are included in Fig. 4b. From the HRTEM micrograph of InP@ZnS sample synthesized at 320 °C, it is clearly observed the formation of nanocrystals with a well-defined crystalline structure. Amplifying and analysing the selected area of the micrograph (it is shown in Fig. 4b), it was possible to calculate the interplanar distances of 3.3 Å corresponding to plane (111) of particles of crystallized InP in crystalline phase zinc-blende type. On the other hand, in Fig. 4c is shown as reference the HRTEM micrograph of ZnS nanoparticles, the analysis shows the crystalline structure of the particle and an interplanar distance of 4.5 Å corresponding to plane (101) of ZnS zinc-blende type. As is observed in HRTEM micrograph of InP@ZnS sample shown in Fig. 4b, the presence of ZnS shell on the InP-core is not detected, although it analysed several HRTEM micrographs trying to observe its presence. This suggests that the ZnS shell is very thin so it cannot be detected by HRTEM measurements; as has been reported it is of 5–10 atomic layers, which confirms the results obtained by X-ray diffraction and Raman scattering. The average size of the nanoparticles was obtained with TEM micrographs, which are presented in Table 2, along with the results obtained with the Wang equation and the Debye–Scherrer equation. These results show good agreement and the observed differences are due to the approximations used, mainly at high temperatures.

Since with the experimental techniques discussed above the presence of the ZnS shell on InP-core could not be detected, PL measurements at room temperature of the nanocrystals were performed to study the effect of the synthesis temperature and to be able to detect the ZnS shell. In order to find the suitable precursor concentrations for the synthesis of the nanocrystals, the effect of precursors atomic ratio (In:P:Zn:S = 1:1:0.5:0.5, 1:1:1.5:1.5, 1:1:1:1) on the formation of the ZnS shell on the InP core was investigated by PL, maintaining the synthesis temperature at 280 °C. The room temperature PL spectra for the three precursor atomic ratios are shown in Fig. 5, which show two well-resolved radiative bands that are constituted by three bands centred at 2.22, 2.52 and 2.99 eV. The first one is associated with the InP-core, which is dominant and the other two are associated with the ZnS-shell [11, 34], which will be discussed more widely later. As is seen from the PL spectra, the height

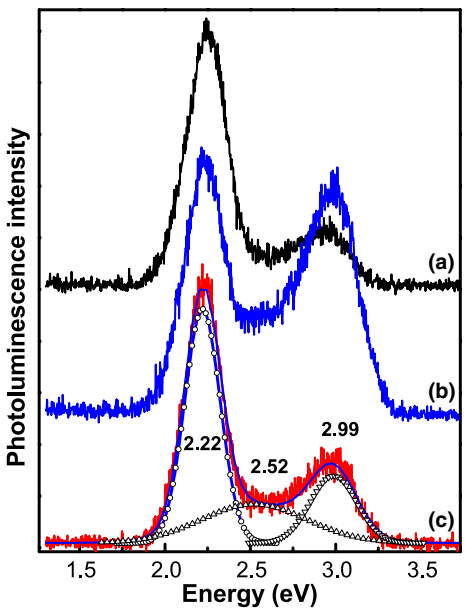

Fig. 5 It is shown the PL spectra of three samples synthetized at 280 °C during 2 h with different precursor atomic ratios (In:P:Zn:S); *a* (1:1:0.5:0.5), *b* (1:1:1.5:1.5) and *c* (1:1:1:1)

of the dominant peak and the full width at half maximum (FWHM) depend on the concentration of precursors. Obtaining better results for atomic ratio In:P:Zn:S = 1:1:1:1, so it was the concentration of precursors that was taken for all the other experiments that were performed and then they are discussed and analysed. The temperature to synthetize the InP@ZnS nanocrystals was varied over a wide range and its effect on them was also studied by means of room-temperature PL measurements. Figure 6 shows the normalized PL spectra of the six different-sized InP@ZnS samples investigated under 325 nm excitation. For the semiconductor nanocrystal sizes of 2.7–3.6 nm, strong emission bands at 2.62–2.17 eV were observed. This grain size-dependence PL is a direct consequence of the quantum-confinement effect actives on the InP-core NCs, namely on their exciton transitions. As is observed in Fig. 6, the absence of radiative transitions in the ZnS-shell is quite questionable, particularly when exciting the InP@ZnS NCs with light of wavelength lower than 400 nm. In such a case, the corresponding excitation photon energy is well above the transition energy of the InP-core NCs and high enough to excite ZnS shell trap states generated from lattice imperfections like Zinc-vacancy or certain donors. The self-activated (SA) radiative band peaking at ~ 2.94 eV is well known in ZnS [35]. It originates from the recombination of donor–acceptor pairs, in which the donor is usually generated from the replacement of S by a Group-VII atom or the replacement of Zn by a Group-III atom, while the acceptor is preferably the Zn-vacancy. The SA band in bulk ZnS crystals is excited efficiently by 365 nm photons [35]. On the other hand, the ZnS-shell on the InP-core resulted in a strong increase of the PL intensity of the InP NCs, which is attributed to the passivation of their surface states and quantum confinement of the photogenerated carriers inside the InP core. For sample M1, which was synthesised at 100 °C, along with the radiative band originating from the exciton transition in the InP-core of the NCs at 2.62 eV, one can see other PL band peaking at energies around 1.76, 2.94 and 3.21 eV. The latter two radiative signals are very similar in difference ZnS NCs systems, regardless of the size of InP-core NCs. Therefore, the radiative band at 3.21 eV (UV band) corresponds to the direct de-excitation from the O_T levels to valence band (VB), the radiative band observed at 2.94 eV (blue) is associated a transition from *CB-to-*I_S. Finally, the radiative band at 1.76 eV could be associated to a radiative transition of defect levels of interstitial sulphur to valence band. In fact, ZnS single crystals emit intensive blue luminescence under excitation with the 365 nm line [36]. The 365 nm light is below the band gap of ZnS; however, it can excite defect-related centres like SA to emit luminescence. Therefore, the PL spectrum of the sample M1 could be interpreted that InP NCs are formed but are not fully covered by the ZnS-shell. Additionally, the full width at half-maximum (FWHM) band InP NCs is very wide, ~ 348.5 meV. Indicating a high density of surface states and possibly an inhomogeneity grain size of InP NCs. As the synthesis temperature is increased, the radiative bands associated with the ZnS-shell disappear and only predominate the band assigned to the InP-core. The radiative weak band to its left at 2.30 eV that could be originated in InP cores associated to radiative transition CB-to-I_p, which disappears with the increase of the temperature since the InP@ZnS NCs become stoichiometric, see Table 1. In addition, as the synthesis temperature is increased the PL intensity increases strongly, see Fig. 7. The FWHM decreases appreciably up to 177.8 meV at 300 °C, indicating that the density of surface states decreases drastically by passivation due to the ZnS-shell formation, which is shown in inset of Fig. 7. As is observed in Fig. 6, the RT-PL spectra in all the used synthesis temperatures only the excitonic band is dominant and besides this is redshifted and its FWHM diminishes, which is indicative that nanocrystal size increases and the ZnS shell cover InP-core completely. On the other hand, the FWHM of the radiative band of InP@ZnS NCs decreases slightly with increasing temperature from 348.5 to 177.8 meV at 300 °C, which is shown in inset of Fig. 7. The RT-PL intensity increases, indicating a high passivation of the NCs due the ZnS shell completely covers the InP core, and this could be between 5 and 10 atomic layers [21]. Because of if it has a greater number of atomic layers the luminescence intensity decreases, which could be the origin of the luminescence at temperatures of synthesis higher than 300 °C decreases and its FWHM increases. This is indicative that higher temperatures increases the number

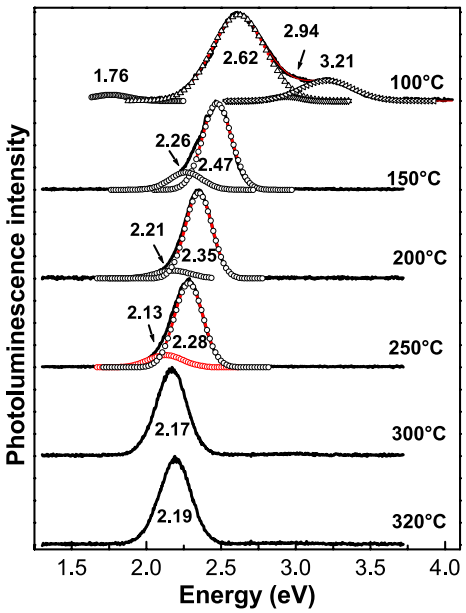

Fig. 6 It shows the 300 K PL spectra of the InP@ZnS NCs synthetized at different temperatures

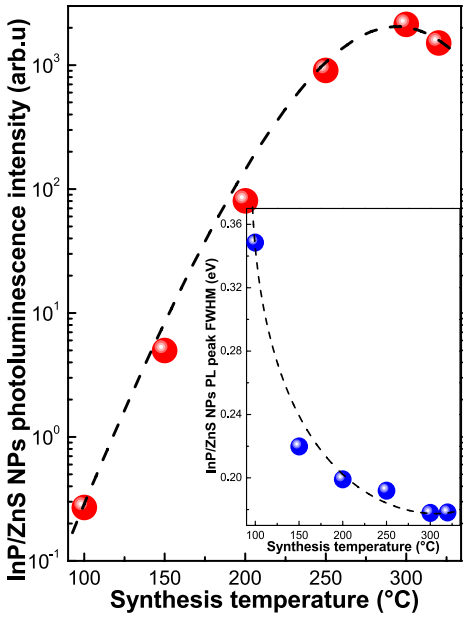

Fig. 7 It is shown the graph of the PL intensity of the InP@ZnS NCs synthetized as a function of the synthesis temperature, which shows a high passivation. In the inset is shown the FWHM of the PL peak of the InP@ZnS nanocrystals as a function of the synthesis temperature

of atomic layers, damaging the optical properties of InP@ZnS NCs.

4 Conclusions

InP@ZnS nanocrystals of were successfully synthesised by the colloid chemistry method at different synthesis temperatures. Temperature-dependent physical and chemical properties of ZnS-shell formation were studied using different characterization techniques. The crystalline phase of InP-core was zinc blende type centred on the face that was found by X-ray diffraction and Raman spectroscopy, which was confirmed by HRTEM. By varying the synthesis temperature from 100 to 320 °C, semiconductor nanocrystals were obtained with a diameter ranged from 3 to 7 nm, which were obtained by room temperature absorbance measurements through the Wang equation. These values were confirmed by TEM measurements and X-ray diffraction. It was found that PL increases with the synthesis temperature due to the passivation of surface states, which suggests the formation of the ZnS-shell on the InP-core. At the synthesis temperature of 300 °C the best passivation results are obtained, which means that the ZnS shell is complete on InP nanocrystal, whose thickness is between 5 and 10 atomic layers. At higher temperatures, the luminescence intensity decreases indicating that the structural quality of the nanocrystals becomes more defective.

Acknowledgements The authors thank SIP-IPN for their support for the development of this work.

References

1. J.H. Park, J.Y. Kim, B.D. Chin, Y.C. Kim, J.K. Kim, O.O. Park, Nanotechnology **15**, 1217 (2004)
2. E. Katz, I. Willner, *Nanobiotechnology-Concepts, Applications and perspectives*, Chap. 14 ed. by C.M. Niemeyer, C.A. Mirkin (Wiley-VCH, Weinheim, 2004), pp. 200–226
3. V.L. Colvin, M.C. Schlamp, A.P. Alivisatos, Nature **370**, 354 (1994)
4. R. Rossetti, J.L. Ellison, J.M. Gibson, L.E. Brus, J. Chem. Phys. **80**, 4464 (1984)
5. D. Vasudevan, R.R. Gaddam, A. Trinchi, I. Cole, J. Alloys Compd. **636**, 395 (2015)
6. A.D. Dinsmore, D.S. Hsu, H.F. Gray, S.B. Qadri, Y. Tian, B.R. Ratna, Appl. Phys. Lett. **75**, 802 (1999)
7. R. Maity, K.K. Chattopadhyay, Nanotechnology **15**, 812 (2004)
8. J. Tittel, W. Gohde, F. Koberling, T. Basché, A. Kornowski, H. Weller, A. Eychmüller., J. Phys. Chem. B **101**, 3013 (1997)
9. S. Mahamuni, K. Borgohain, B.S. Bendre, V.J. Leppert, S.H. Risbud, J. Appl. Phys. **85**, 2861 (1999)
10. A.L. Rogach, Mater. Sci. Eng. B **69/70**, 435 (2000)
11. J.P. Borah, J. Barman, K.C. Sarma, Chalcogenide Lett. **5**, 201 (2008)
12. J. Park, J. Joo, S.G. Kwon, Y. Jang, T. Hyeon, Angew. Chem. **46**, 4630 (2007)
13. S. Tamang, C. Lincheneau, Y. Hermans, S. Jeong, P. Reiss, Chem. Mater. **28**, 2491 (2016)
14. M. Levinshteĭn, S. Rumyantsev, M. Shur, *Schmidt Handbook Series on Semiconductor Parameters*, vol. 1 (World Scientific, London, 1996)
15. E. Koroknay, W.-M. Schulz, M. Eichfelder, R. Roßbach, M. Jetter, P. Michler, J. Phys. Conf. Ser. **245**, 012077 (2010)
16. H. Okuda, J. Takada, Y. Iwasaki, N. Hashimoto, C. Nagao, IEEE Trans. Consum. Electr. **36**, 436 (1990)
17. J. Ghrayeb, T.W. Jackson, R. Daniels, D.G. Hopper, In AeroSense '97, p. 237 (1997)
18. J.C. Barton, P.W. Ranby, J. Phys. E **10**, 437 (1977)
19. A.Z. Obidin, A.N. Pechenov, Yu.M. Popov, V.A. Frolov, Yu.V. Korostelin, P.V. Shapkin, Sov. J. Quantum Electron. **18**, 1100 (1988)
20. L. Li, P. Reiss., J. Am. Chem. Soc. **130**, 11588 (2008)
21. A.D. Lad, S. Mahamuni, Phys. Rev. B **78**, 125421 (2008)
22. M.J. Seong, O.I. Mićić, A.J. Nozik, A. Mascarenhas, H.M. Cheong. Appl. Phys. Lett. **82**, 185 (2003)
23. V.K. LaMer, R.H. Dinegar, J. Am. Chem. Soc. **72**, 4847 (1950)
24. M. Green, Curr. Opin. Solid State Mater. Sci. **6**, 355 (2002)
25. L.C. Hernández, L. Ponce, E. Rodríguez, A. Fundora, G. Santana, J.L. Menchaca, E. Pérez-Tijerina, Nanoscale Res. Lett. **7**:80 (2012)
26. P. Reiss, M. Protière, L. Li, Small **5**, 154 (2009)
27. M.R. Loghman-Estarki, M. Hajizadeh-Oghaz, H. Edris, R.S. Razavi, CrystEngComm. **15**, 5898 (2013)
28. M. Mohammadikish, F. Davar, M.R. Loghman-Estarki, Z. Hamidi, Ceram. Int. **39**, 3173 (2013)
29. F. Davar, M.R. Loghman-Estarki, R. Ashiri, J. Ind. Eng. Chem. **21**, 965 (2015)
30. J.P. Kim, J.A. Christians, H. Choi, S. Krishnamurthy, P.V. Kamat, J. Phys. Chem. Lett. **5**, 1103 (2014)
31. A.D. Yoffe, Adv. Phys. **42**, 173 (1993)
32. Y. Wang, A. Suna, W. Mahler, R. Kasowski., J. Chem. Phys. **87**, 7315–7322 (1987)

33. Y. Wang, X. Yang, T.C. He, Y. Gao, H.V. Demir, X.W. Sun, H.D. Sun, Appl. Phys. Lett. **102**, 021917 (2013)
34. J. Díaz-Reyes, R.S. Castillo-Ojeda, R. Sánchez-Espíndola, M. Galván-Arellano, O. Zaca-Moran, Curr. Appl. Phys. **15**, 103 (2015)
35. N.Q. Liem, V.X. Quang, D.X. Thanh, Acta Phys. Pol. A **86**, 979 (1994)
36. C. Unni, D. Philip, K.G. Gopchandran, Opt. Mater. **32**, 169 (2009)